CHEMICAL VAPOR DEPOSITION TECHNIQUES FOR THIN FILMS OF SOLID ELECTROLYTES AND ELECTRODES

V.E.J. van DIETEN, J.P. DEKKER, A.A. van ZOMEREN, and J. SCHOONMAN
Laboratory for Applied Inorganic Chemistry
Delft University of Technology
Julianalaan 136
2628 BL Delft
The Netherlands

ABSTRACT. Chemical Vapor Deposition (CVD) is a promising technology for the fabrication of thin films for components of solid state electrochemical devices. Electrochemical Vapor Deposition (EVD) is a special CVD technique for the production of thin gas impervious films of the solid electrolyte, Yttria Stabilized Zirconia (YSZ) for Solid Oxide Fuel Cells (SOFC's). The kinetics of the film growth of YSZ can be modeled considering the Wagner oxidation process and thermodynamic equilibrium at the gas-solid interphases. The calculated thermodynamic equilibrium can be used to predict the film growth rate. The results show that the EVD growth of YSZ is most likely governed by defect transport in the EVD layer, and a mass transfer limitation at the surface on the metal chloride side. Metal Organic Chemical Vapor Deposition (MOCVD) has been used for the fabrication of thin-film TiS_2 cathodes for rechargeable batteries. The OCV of TiS_2|1M $LiClO_4$ in PC|Li batteries, and the chemical diffusion coefficient and thermodynamic enhancement factor have been determined as a function of lithium content in these films. Electrochemical measurements include GITT and Impedance Spectroscopy on the cell TiS_2|1M $LiClO_4$ in PC|Li. The influence of the MOCVD conditions on the deposition rate and morphology has been investigated. The morphology of the films seems to be independent of temperature and pressure, in the temperature range from 250°C to 450°C and total pressures of 7.5 and 20 mbar, and preferred orientation of the TiS_2 crystallites.

1. Introduction

In recent years there has been an enormous increase in the application of thin film technologies in the fabrication of solid state electrochemical devices. Thin film technologies offer the possibility to miniaturize devices and to decrease their internal resistance by minimizing the thickness of the individual components. Devices in which thin film components are utilized are e.g. Solid Oxide Fuel Cells (SOFC's),

B. Scrosati et al. (eds.), Fast Ion Transport in Solids, 231–257.

thin film rechargeable batteries, and chemical gas sensors.

Chemical vapor deposition (CVD) is one of the synthesis techniques for the fabrication of thin film components for solid state electrochemical devices. This paper will focus on two CVD techniques; i.e. for the fabrication of the solid electrolyte of SOFC's, and for the cathode of rechargeable lithium batteries.

A SOFC is a device in which the free energy of a chemical reaction is converted directly into electrical energy, so it has the advantage of not being Carnot limited. High fuel efficiency and potentially very large power density are therefore possible. To develop high energy density SOFC's, its weight and internal resistance must be minimized.

There are three major types of SOFC's, i.e. the tubular, the monolithic, and the planar type. The ohmic polarization losses are dependent on the cell design. For the thin-film tubular SOFC configuration developed by Westinghouse the contribution of the individual components to the total cell resistance is given in Table 1 [1]. Although the electrodes have low specific resistivities in comparison with the solid electrolyte and the interconnection material, they produce the largest polarization loss because of the relatively long current pathways. To minimize the ohmic polarization losses, the components should be as thin as possible, while maintaining their other required properties.

Although the contribution to the total cell resistance is small in the tubular design, the fabrication of thin gas tight films of the solid electrolyte yttria stabilized zirconia (YSZ) has attracted widespread attention. For the synthesis of thin dense films of YSZ, Electrochemical Vapor Deposition (EVD) has become a key technology. In order to obtain a better understanding of the growth kinetics of the EVD process, the experimental data on the growth of YSZ by means of EVD have been collected, and a systematical comparison has been made. To explain the observed growth rates,

TABLE 1. Contribution of the individual components of a tubular SOFC to the total cell resistance.

Component	R (1000°C) (Ω cm)	Thickness (mm)	Contribution to cell resistance (%)
cathode ($La_{1-x}Sr_xMnO_{3-\delta}$)	0.013	0.07	65
anode (Ni-ZrO_2)	0.001	0.10	25
electrolyte ($Zr_{1-x}Y_xO_{2-x/2}$)	10.0	0.04	9
interconnect ($LaCr_{1-x}Mg_xO_{3-\gamma}$)	0.5	0.04	1

the kinetics of the EVD growth of YSZ have been modeled using the Wagner oxidation theory, and the thermodynamic equilibrium at the gas/solid interphases.

By miniaturizing solid state batteries, they can be integrated with electronic circuits, and either the current or the voltage can easily be amplified by connecting the batteries either parallel or in series.

Solid state lithium cells have the advantage of a high energy density, low self discharge and a long shelf life. This makes them especially suitable for low-power microelectronic devices such as read/write memories. One of the problems of the lithium batteries is the current density. This depends on the respective rates of the electrochemical processes in the cell. Diffusion of lithium into the insertion cathode appears to be one of the limiting factors. The advantage of a thin-film lithium battery is that the diffusion pathway for lithium is short.

Titanium disulphide (TiS_2) is a well-known cathode material for rechargeable lithium batteries, because of its good ionic and electronic conductivity. Hexagonal TiS_2 has a layered structure with weak VanderWaals bonding between the layers. Lithium can easily be inserted between these layers. The lithium conduction of TiS_2 is anisotropic, so cells can suffer from polarization losses due to random crystallite orientation. These losses may be reduced by depositing the TiS_2 layers with a preferred crystallite orientation. In monocrystalline Li_xTiS_2 the chemical diffusion coefficient of lithium is on the order of 10^{-8} - 10^{-9} cm^2/s. In microcrystalline layers, synthesized by means of CVD, the chemical diffusion coefficients appear to be much smaller: 1.1×10^{-11} - 4×10^{-13} cm^2/s [2]. In this case the highest diffusion coefficient was obtained in layers with a preferred orientation with the c-axis parallel to the substrate surface.

Metal Organic Chemical Vapor Deposition (MOCVD) is used to deposit cathode layers of TiS_2 with increased lithium diffusion coefficients, because it offers the possibility of good microstructural control. The electrochemical properties of some TiS_2 films have been determined.

First, the principle of CVD will briefly be discussed, as well as the principles of the EVD and MOCVD processes.

2. Chemical Vapor Deposition Techniques

2.1 CHEMICAL VAPOR DEPOSITION

CVD is a process for the synthesis of solid products by chemical reactions between gaseous reactants. With CVD, high temperature materials, such as ceramics or refractory metals, are formed at moderate reaction temperatures. The reaction temperature lies well below the melting point of the product. The materials can be synthesized in the form of coatings, powders or formed solid products [3-6].

Powder synthesis is in volume the largest application of CVD. With CVD it is possible to produce uniform particles of ultra high purity. E.g. titanium dioxide

pigment, and highly sinterable silicon nitride powder are produced by CVD [7,8].

Conventional CVD is used to form wear, erosion and corrosion resistant coatings of e.g. titanium nitride, titanium carbide, silicon carbide or cubic boron nitride [3-6, 9-13]. The CVD process is also used extensively in microelectronics, optics and superconductivity research [14, 15].

Many different chemical reactions occur in CVD processes, i.e. thermal decomposition reactions, oxidation and reduction reactions, nitridation, boronation, and carburation reactions. The composition and properties of the product can be controlled by the process parameters, which are deposition temperature, reactor pressure, gas flow rates, reactant concentrations and reactor geometry. Each CVD process occurs by a number of sequential steps, which can be summarized as follows [16]:

1) Transport of the reactants to the reaction zone.
2) Diffusion of the reactants to the substrate surface, through a stagnant boundary layer.
3) Adsorption of species on the substrate surface.
4) Chemical reaction at the substrate surface.
5) Desorption of volatile reaction products from the substrate surface.
6) Diffusion of the volatile reaction products through the stagnant boundary layer.
7) Transport of the waste products to the reactor outlet.

It is also possible that homogeneous reactions in the gas phase occur. Powders are formed by means of homogeneous nucleation, but also gaseous products can be formed.

At least one of these steps may determine the overall deposition rate, and each step depends in a different way on the experimental parameters. An understanding of the growth kinetics of a CVD process is necessary in order to be able to control the process.

Nowadays there are many different types of CVD techniques. The names used for these techniques refer to the most important aspect of the process, in which it deviates from the conventional CVD process.

In conventional CVD the reactants are thermally activated, either in a hot- or cold-wall reactor. Substrate temperatures are generally high (above 600°C). If the substrates used can not withstand these high temperatures, more advanced CVD techniques, such as Laser-CVD (LCVD) or Plasma Enhanced CVD (PECVD), have to be used, or the nature of the reactants has to be altered, particularly by using organometallic compounds (MOCVD).

In LCVD the reactants can be activated thermally using an IR-laser, or chemical bonds can be selectively broken using a UV-laser. In PECVD the activation energy for the reactions is provided by a glow discharge in the vicinity of the substrate. This allows the deposition to occur at temperatures lower than those required for conventional CVD.

In Low-Pressure or Atmospheric-Pressure CVD (LP- or APCVD) the name refers

to the reaction pressure. In EVD [17-24] and Particle Precipitation aided CVD (PPCVD) [25,26] the name refers to the type of chemical process. In Fluidized Bed CVD (FBCVD) [27], and Hot Filament CVD (HFCVD) [28], it refers to the reactor type used.

In the field of fabrication of thin films for solid state electrochemical devices EVD and MOCVD are the preferred technologies. The principles of these processes will be briefly discussed below.

2.2 ELECTROCHEMICAL VAPOR DEPOSITION

2.2.1 *Principle of the process.* EVD is a modified form of CVD, developed by Westinghouse, which utilizes a chemical potential gradient to grow thin, gas impervious layers of either electronically, or ionically conducting metal oxides on porous substrates [17-24]. The primary application of EVD to date has been in the fabrication of the solid electrolyte YSZ, and the interconnection material magnesium-doped lanthanum chromite as used in SOFC's.

The steps involved in the EVD process are shown in figure 1. A porous substrate separates the reactant metal chloride vapors from a mixture of oxygen (O_2) and steam (H_2O). The first step in film formation involves pore closure by a normal CVD-type reaction between the reactant metal chloride and steam (or oxygen).

$$MeCl_4\ (g) + 2\ H_2O\ (g) \rightarrow MeO_2\ (s) + 4\ HCl\ (g) \qquad (1)$$

Once pore closure is complete, the reactants are no longer in direct contact. Film growth then proceeds by oxygen ion diffusion through the film due to the presence of a large oxygen chemical potential gradient across the deposited film.

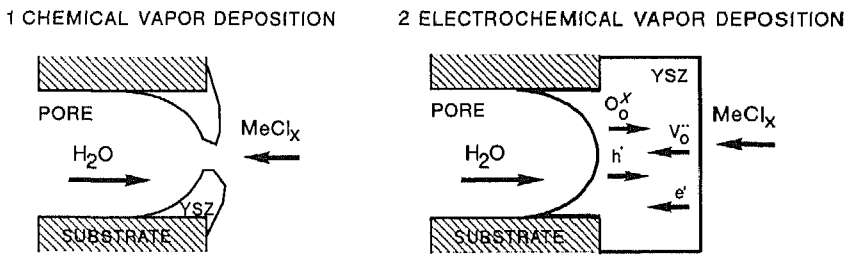

Figure 1. The principle of the two stages of the EVD process. The diffusion processes during the EVD growth of YSZ are also shown.

In this step oxygen ion vacancies and electrons formed at the metal chloride side diffuse through the thin metal oxide layer to the oxygen-rich side. This results in a net flux of oxygen to the metal chloride side, where the oxygen reacts with the metal chloride vapor to form the metal oxide product.

$$MeCl_4\ (g) + 2\ O_O^x \rightarrow MeO_2\ (s) + 4\ e' + 2\ V_O^{\cdot\cdot} + 2\ Cl_2\ (g) \qquad (2)$$

The pore closure step is very important in determining the ultimate properties of the deposited film. Ideally, the pore plugging layer (CVD layer) should form on the substrate surface at the metal chloride side, and barely penetrate the substrate pores, be thin and as close to the composition of the EVD layer as possible.

2.2.2 *Solid state transport in EVD layers.* The overall film growth can be limited by a) gas diffusion, b) surface kinetics on either side of the film, or c) solid state diffusion in the growing film. When the rate of film growth is controlled by solid state diffusion the kinetics are similar to the Wagner oxidation of metals. In Wagner oxidation the rate of film growth is inversely proportional to the oxide thickness [29,30].

$$\frac{dL}{dt} = \frac{K_0}{L} \qquad (3)$$

The integrated form of equation (3) yields the parabolic rate law.

$$L^2 = 2\ K_0 t + C_0 \qquad (4)$$

Here K_0 is the parabolic rate constant, L the film thickness, t the total deposition time of the second step (EVD growth), and C_0 a constant of integration.

This equation has been used to verify as to whether EVD growth of YSZ is controlled by solid state diffusion. The film growth data in the literature have been fitted according to equation (4) [17-24]. The fitted growth rate constants from these experimental data have been used for further analysis of the EVD process [31].

The diffusion processes which take place during EVD growth of YSZ are also shown schematically in figure 1. Oxygen ion diffusion is only possible if at the same time a counterdiffusion of a species with the same charge or a parallel diffusion of a species with opposite charge occurs to preserve electroneutrality. In YSZ metal ion

diffusion can be neglected.

When solid state diffusion in the growing film is rate limiting the reactions at the gas/solid interphases are considered to be rapid such that thermodynamic equilibria at these interphases are established. The oxygen partial pressures on either side of the film are determined by the thermodynamic equilibria.

In terms of ionic flux (j_i) the growth rate can be expressed as [30]:

$$\frac{dL}{dt} = \frac{2}{z} j_i V_m \tag{5}$$

Here z is the total cation charge, V_m is the molar volume of the growing oxide.

For an ionically conducting material the general expression for the ionic flux is given by,

$$j_i = -\{\frac{RT}{2CF^2}\int_{P_{O_2}}^{P'_{O_2}} \sigma_{el}\, d \ln P_{O_2}\}\ \frac{1}{\Delta L} \tag{6}$$

where R is the gas constant, T the absolute temperature, C the total anion charge per equivalent of YSZ (i.e. 3.82 for 10 m/o YSZ), F the Faraday constant, σ_{el} the total electronic conductivity, P_{O2} the oxygen partial pressure on the water side and P'_{O2} the oxygen partial pressure on the metal chloride side. From equations (5) and (6) the parabolic growth rate can be derived to yield [17-24],

$$K_0 = \frac{R\,T\,V_m}{C\,F^2}\,(\sigma_p^0\,(P_{O_2}^{1/4} - (P'_{O_2})^{1/4}) + \sigma_n^0\,((P'_{O_2})^{-1/4} - P_{O_2}^{-1/4})) \tag{7}$$

where σ_p^0 is the electron hole conductivity at an oxygen activity of one, and σ_n^0 the electron conductivity at an oxygen activity of one. Substituting values expected to be typical for EVD experiments, i.e. low oxygen partial pressures, in equation (7) reveals that this equation can be simplified to (8).

$$K_0 = \frac{RTV_m}{CF^2}\,\sigma_n^0\,(P'_{O_2})^{-1/4} \tag{8}$$

It should be noted that this equation can only be valid as long as the oxygen

partial pressure is low enough to maintain an electron controlled semiconductivity in YSZ.

Equation (8) can be used to calculate the parabolic growth rate constant provided the oxygen partial pressure on the metal chloride side and the electron conductivity are known as a function of temperature and oxygen partial pressure.

An expression for the electron conductivity of YSZ as a function of its surrounding atmosphere can be derived. Assuming that all defects are fully ionized, the defect reaction for YSZ can be written as (9).

$$Y_2O_3 \rightarrow 2\ Y'_{Zr} + 3\ O_O^x + V_O^{\cdot\cdot} \tag{9}$$

Hence, the oxygen ion vacancy concentration is determined by the dopant concentration of yttria. The following non-stoichiometric defect reaction for YSZ at low oxygen partial pressures can be written [32]:

$$O_O^x \rightleftharpoons 2\ e' + V_O^{\cdot\cdot} + \frac{1}{2}\ O_2\ (g) \tag{10}$$

The equilibrium constant K_{10} for this reaction is given by,

$$K_{10} = [V_O^{\cdot\cdot}]\ [e']^2\ P_{O_2}^{1/2} \tag{11}$$

where $[V_O^{\cdot\cdot}]$ is the concentration of fully ionized oxygen ion vacancies in the oxygen sub-lattice, and $[e']$ the electron concentration in the conduction band.

Thus, at a given dopant concentration and temperature, the concentration of electrons is determined by the partial pressure of oxygen.

The electron conductivity is given by [30],

$$\sigma_n = [e']\ |q|\ \mu_n \tag{12}$$

where q is the electronic charge, and μ_n the electron mobility. If the mobility is independent of the electron concentration the electron conductivity is proportional to the electron concentration. Assuming that the equilibrium in reaction (10) is present, an expression for the electron conductivity can be obtained by combining equations (11) and (12).

$$\sigma_n = \frac{|q|\mu_n}{[V_O^{\cdot\cdot}]^{1/2}} K_{10}^{1/2} P_{O_2}^{-1/4} \qquad (13)$$

Equation (13) is proportional to $P_{O2}^{-1/4}$. Also other sets of defect reactions, involving electrons and oxygen ion vacancies, instead of reaction (10) can be used to obtain an expression for the electron conductivity. These expressions will always contain a product of several equilibrium constants and $P_{O2}^{-1/4}$. Each of these products of equilibrium constants is equal to the square root of equilibrium constant K_{10} [33]. Equation (13) can be combined with equation (8) to obtain an expression for the parabolic growth rate constant.

2.2.3 *Thermodynamics.* P'_{O2} is determined by the thermodynamic equilibrium of the species present at the metal chloride side. The assumption that a gas phase thermodynamic equilibrium is present, is justified as long as the solid state diffusion is rate limiting, and all other reaction rates are infinite. Thermodynamic equilibria can be computed with the SOLGASMIX and Chemsage programs [34,35]. The thermochemical data of the species necessary for these calculations are obtained from the JANAF Tables [36].

In order to calculate the parabolic growth rate constant from equation (8), the electron conductivity as a function of the metal chloride containing atmosphere has to be known. In principle this information can be obtained from thermodynamic calculations provided the thermochemical data of the individual defects in YSZ are known. Since such data are not available these calculations can not be executed. Hence, the electron conductivity σ_n, as a function of oxygen partial pressure, has to be obtained from conductivity data of YSZ from literature [32]. The oxygen partial pressure has to be calculated from the thermodynamic equilibrium at the gas/solid interphase.

For simplicity only the presence of zirconium containing species will be considered in the following discussion. The actual equilibrium between $ZrCl_4$ and ZrO_2 (i.e. the EVD film of YSZ) is given by (14).

$$ZrCl_4\ (g) + 2\ O_O^x \rightleftharpoons ZrO_2\ (s) + 4\ e' + 2\ V_O^{\cdot\cdot} + 2\ Cl_2\ (g) \qquad (14)$$

Equilibrium constant of equilibrium (14) can be expressed as a function of oxygen partial pressure by incorporating the equilibrium of $ZrCl_4$ with oxygen, i.e.

$$ZrCl_4\ (g) + O_2\ (g) \rightleftharpoons ZrO_2\ (s) + 2\ Cl_2\ (g) \qquad (15)$$

The actual partial pressure of oxygen can be governed by several parameters, depending on experimental conditions which affect the partial pressures in reaction (15).

As long as the conversion of reactant in the EVD process is relatively low, P'_{O2} can be determined, provided the partial pressure of chlorine is known. Chlorine is not an input species, but it is a product formed by some chemical reaction. So the partial pressure of chlorine will be determined in one of the following ways:

(a) by the conversion of metal chloride reactant at the metal oxide surface. However, this partial pressure of chlorine is determined by the growth rate of the film itself and is dependent of several mass transport processes such as adsorption and desorption and gas phase diffusion. This complex set of mass transport processes makes it very difficult to obtain realistic values of the chlorine partial pressure,

(b) by the dissociation of $ZrCl_4$.

$$3\ ZrCl_4(g) \rightleftharpoons \sum_{n=1}^{3} \left(ZrCl_n(g) + (4-n)\left(\frac{(1-a)}{2}\ Cl_2(g) + a\ Cl(g)\right)\right)\ a \in [0,1] \qquad (16)$$

Because the equilibrium in reaction (15) still holds , P'_{O2} can be calculated from this equilibrium,

(c) by the presence of oxygen in the carrier gas stream. This will have a major influence on the partial pressures of the species present in equilibrium (15).

Cases (b) and (c) can be studied by calculation of the thermodynamic equilibrium present in the gas phase on the metal chloride side.

The thermodynamic equilibria have been computed as a function of temperature and partial pressures of the input species [37]. The total pressure was kept constant at 0.01 atm through all calculations. Using the results of these calculations, values for the parabolic growth rate constant have been calculated. Finally, these calculated growth rate constants have been compared with the fitted growth rate constants from the experiments and the results will be discussed.

2.3 METAL ORGANIC CHEMICAL VAPOR DEPOSITION

The main characteristic of the MOCVD process is the use of organometallic compounds as the source for the metal ions. The organometallic compounds are usually volatile, and the bonding between the metal and non-metal atoms is relatively weak. Hence, in comparison with the conventional CVD process, generally lower

substrate temperatures are required. Furthermore, there are no extremely hot and corrosive gases present in the reactor. A disadvantage of the process, for non-carbides and non-oxides, is the possible incorporation of carbon or oxygen into the deposits.

A typical (MO)CVD system is outlined in figure 2. It contains a gas delivery system with a purification section and gas flow controllers. Part of the carrier gas stream can be passed through a reflux evaporator, in case a liquid reactant is used, or a solid compound evaporator, in case of a solid reactant. The gas stream can either be mixed in a mixing chamber, or be fed directly into the reactor. Experiments can be performed in a hot- as well as a cold-wall reactor. The waste gases are passed through a liquid nitrogen trap, to protect the pump unit, which is used to establish low pressures.

TiS_2 has already been synthesized by CVD using titanium tetrachloride ($TiCl_4$) and dihydrogen sulphide (H_2S) at temperatures ranging from 300 to 1000°C [2]. By using hexamethyldisilathiane (HMDST) instead of H_2S as the sulphur precursor, it might be possible to lower the deposition temperature [38]. TiS_2 is formed by the following reaction:

$$TiCl_4\ (g) + 2\ (CH_3)_6Si_2S\ (g) \rightarrow TiS_2\ (s) + organic\ products\ (g) \qquad (17)$$

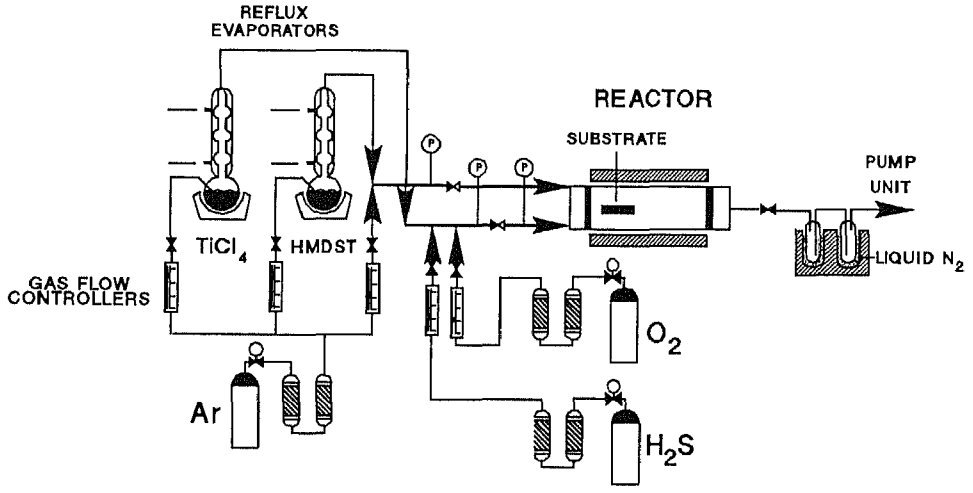

Figure 2. Experimental setup for (Metal Organic) Chemical Vapor Deposition of TiS_2.

Using this reactant, it might be possible that, besides carbon, silicon will be incorporated into the deposit.

The objective is to increase the current exchange area by depositing a smooth TiS_2 film, and to eliminate the influence of crystallite orientation by depositing a three-dimensionally conducting TiS_2 film. Therefore, either an amorphous or a microcrystalline film is needed. If the film is used in combination with a solid electrolyte, it should have no porosity. Because an increase in porosity will result in higher current densities, and this will lead to enhanced polarization at grain boundaries. In amorphous films lithium diffusion may be slower than in crystalline films, because the VanderWaals gaps allow for relatively fast diffusion. However, in a randomly oriented and non-porous microcrystalline film the diffusion coefficient should be 2/3 of that in a single crystal, in the direction perpendicular to the c-axis.

TiS_2 films have been deposited using $TiCl_4$ and HMDST or H_2S as precursors [38]. The depositions were carried out in a hot-, as well as a cold-wall reactor in the temperature range of 200 - 400°C, and at pressures of 7.5 and 20 mbar. The feed gas consisted of 1.4 vol% HMDST and 0.25 vol% $TiCl_4$, or 11 vol% H_2S and 0.38 vol% $TiCl_4$ in argon. The resulting films were analyzed using X-Ray Diffraction (XRD) and Scanning Electron Microscopy (SEM) (JEOL JSM-35). The electrochemical properties of the films were analyzed by Open Circuit Voltage (OCV) and Galvanostatic Intermittent Titration (GITT) [39] measurements using a EG&G/PAR 273 potentiostat/galvanostat, and Impedance Spectroscopy (IS) using a Solartron 1250 frequency response analyzer and a Solartron 1286 Electrochemical Interface. All measurements were performed at room temperature on the cell TiS_2|1 M $LiClO_4$ in Propylene Carbonate|Li [38].

3. Modeling of the EVD growth of YSZ

3.1 THERMODYNAMIC CALCULATIONS

The thermodynamic calculations have been divided into two sections. The first section comprised calculations with only ZrO_2 and $ZrCl_4$ as input species, while a large excess of ZrO_2 with respect to $ZrCl_4$ was chosen in order to prevent depletion of ZrO_2. This set of calculations is used to study the effect of the dissociation of $ZrCl_4$ (case (b)). In figure 3 the equilibrium partial pressures of the main species, with the exception of the input species, because of their large excess, are presented as a function of temperature. The equilibrium partial pressures of all species, with exception of $ZrCl_4$, increase with increasing temperature, indicating that the decomposition of $ZrCl_4$ and ZrO_2(s) becomes more important. The thermodynamic calculations as a function of input amount of $ZrCl_4$ reveal that the equilibrium partial pressures of all species are proportional or inversely proportional to a n-th power of the input amount of $ZrCl_4$ because of its large excess, where n can be 0, 0.5, and 1, respectively. From these results all existing equilibria can be calculated.

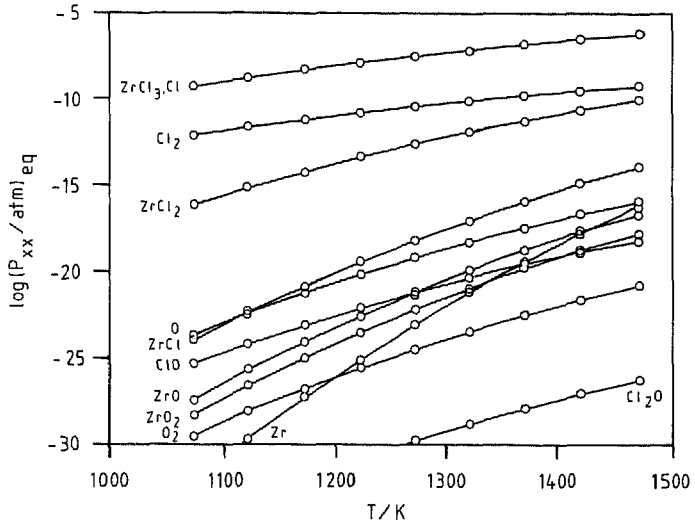

Figure 3. The equilibrium partial pressures P_{xx} of the main species versus temperature, where the input partial pressure of $ZrCl_4$ is 10^{-3} atm, and the input partial pressure of oxygen is kept zero. ZrO_2 is present in large excess.

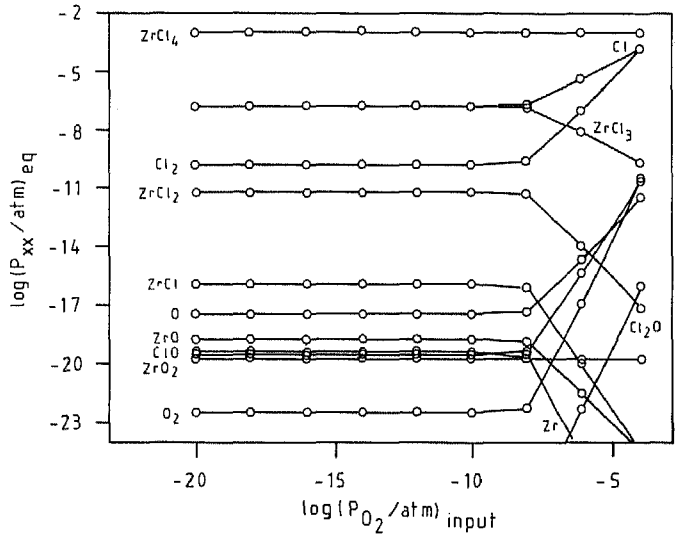

Figure 4. The equilibrium partial pressures P_{xx} of the main species versus the input partial pressure of oxygen at a temperature of 1373 K, where the input partial pressure of $ZrCl_4$ is 10^{-3} atm. ZrO_2 is present in large excess.

The second set of calculations comprised calculations with ZrO_2, $ZrCl_4$, and O_2. This set of calculations is used to study the effect of the presence of oxygen in the input carrier gas. The variation of the input partial pressure of oxygen may have a large influence on the equilibrium partial pressures of the other species. The thermodynamic calculations as a function of temperature reveal that the equilibrium partial pressure of oxygen is high with respect to the equilibrium partial pressure of oxygen for case (b), where no oxygen was taken into account as input species.

The equilibrium partial pressures of the main species as a function of the input partial pressure of oxygen is presented in figure 4. The equilibrium partial pressures of the species are determined by the input amount of $ZrCl_4$ and ZrO_2 as long as the input partial pressure of oxygen is kept below 10^{-8} atm. However, if the input partial pressure of oxygen is above 10^{-8} atm, there is a steep increase in the equilibrium partial pressure of oxygen. From these observations it can be concluded that the presence of oxygen in the carrier gas stream has no influence on the equilibrium partial pressures of the gas phase species provided the oxygen impurity in the carrier gas stream is less than 1 ppm (i.e. 10^{-8} atm in the reactor as calculated).

3.2 REVIEW OF EVD EXPERIMENTS

All the reported data of film thickness as a function of deposition time have been fitted according to equation (4). This equation was chosen to verify as to whether solid state diffusion is the general rate limiting step in the EVD growth of YSZ in

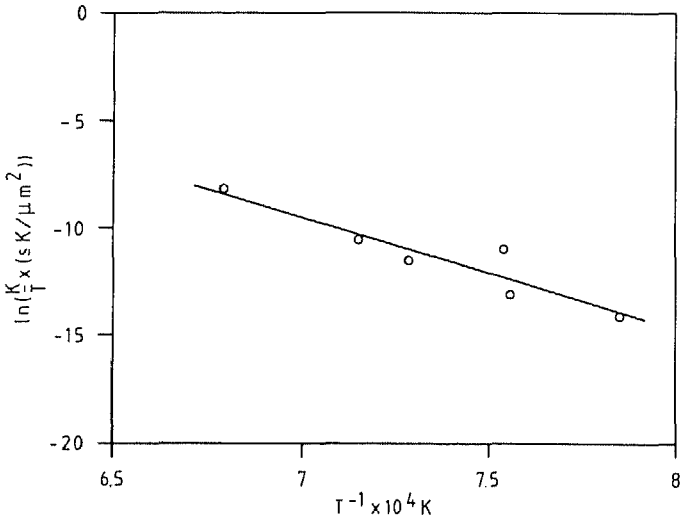

Figure 5. Least squares fit of the parabolic growth rate constant as a function of temperature.

the reported studies [17-24]. In all EVD experiments approximately 8 to 10 m/o yttria was present. All reported EVD experiments could be fitted well by the parabolic growth rate equation (4) [31, 33, 37].

The parabolic growth rate constants are presented as an Arrhenius plot in figure 5. The strong temperature dependence justifies the assumption that the process is indeed controlled by solid state diffusion. The slope of the fitted line is proportional to the apparent activation energy of the process. This apparent activation energy of 4.4 ± 0.7 eV is a direct function of the activation energy for electron conduction in YSZ, and the change in enthalpy of the equilibrium at the metal chloride side, if solid state diffusion is assumed to be rate limiting and all other reaction rates are assumed to be infinite. In this case the apparent activation energy is not directly proportional to the activation energy of electron conduction as was discussed earlier [31].

3.3 MODELING RESULTS OF EVD GROWTH

The parabolic growth rate constants were calculated from equation (8) [31, 37]. The equilibrium oxygen partial pressures were obtained from the calculations where only $ZrCl_4$, ZrO_2, and Ar were used as input species. The results of these calculations for different input concentrations of $ZrCl_4$ are presented in figure 6. The parabolic

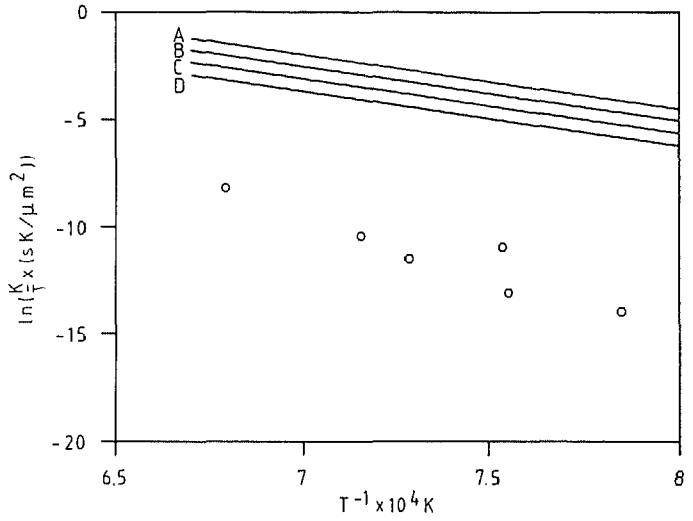

Figure 6. The calculated growth rate constant as a function of temperature, when no oxygen is present as input species. Line A: p_{ZrCl4}(input) = 10^{-6} atm, line B: p_{ZrCl4}(input) = 10^{-5} atm, line C: p_{ZrCl4}(input) = 10^{-4} atm, and line D: p_{ZrCl4}(input) = 10^{-3} atm.

growth rate constant in figure 6 decreases with increasing $ZrCl_4$ input concentration due to the increasing equilibrium partial pressure of oxygen, thereby reducing the chemical potential across the film.

The equilibrium oxygen partial pressures used for the calculation of the parabolic growth rate constants are so low that YSZ is no longer in its electrolytic domain. Hence, the oxygen ion vacancy concentration is not constant anymore. The oxygen ion vacancy concentration and the electron concentration then become proportional to the oxygen partial pressure to the power -1/6 [30]. Thus, the electron conductivity data used are not valid anymore. In this region it is possible that the mass transport in YSZ is determined by the oxygen ion conductivity instead of the electron conductivity.

However, these calculations are still indicative and can still be used to evaluate the experimental data of EVD growth. The predicted parabolic growth rate constant is far too high with respect to the observed parabolic growth rate constant. This discrepancy can not be explained with the fact that YSZ is not in its electrolytic domain anymore, because the calculated parabolic growth rate constant is still far too high in the low oxygen partial pressure limit of the electrolytic domain of YSZ (i.e. $P_{O2} \approx 10^{-23}$ atm).

Yttrium containing species were not considered within the thermodynamic calculations. However, this can not be the explanation for the calculated parabolic growth rate constant being too high, because the calculated equilibrium partial pressure of oxygen becomes lower if yttrium containing species are taken into account due to the formation of yttrium oxychloride (YOCl). This would result in an even higher theoretical parabolic growth rate constant.

Only the metal chloride and metal oxide were considered as input species in the thermodynamic calculations discussed above. However, it is not likely that the carrier gases, argon or helium, used in the experiments are completely free of oxygen. Hence, the influence of small amounts of oxygen in the carrier gas stream on the growth rate has to be investigated.

In order to study the influence of oxygen as an impurity in the carrier gas stream thermodynamic calculations have been performed using O_2, $ZrCl_4$, ZrO_2, and Ar as input species [33,37]. The parabolic growth rate constants were calculated using equation (8). The results of these calculations are presented in figure 7. If the input partial pressure of oxygen drops below 10^{-12} atm the calculated parabolic growth rate constant remains unaffected. The equilibrium partial pressure of oxygen in this case is determined by the input amount of $ZrCl_4$ and ZrO_2. Hence, the parabolic growth rate constant is the same as in the situation where oxygen is not an input species. Thus, line D in figure 6 is equal to lines C, D, and E in figure 7.

The temperature dependence of the calculated parabolic growth rate constant represented by solid line A in figure 7 seems to describe the experimental parabolic growth rate constant reasonably well. This predicted parabolic growth rate constant is obtained using an input oxygen partial pressure of 10^{-4} atm. The calculated apparent activation energy of this parabolic growth rate constant is 3.45 eV [33,37].

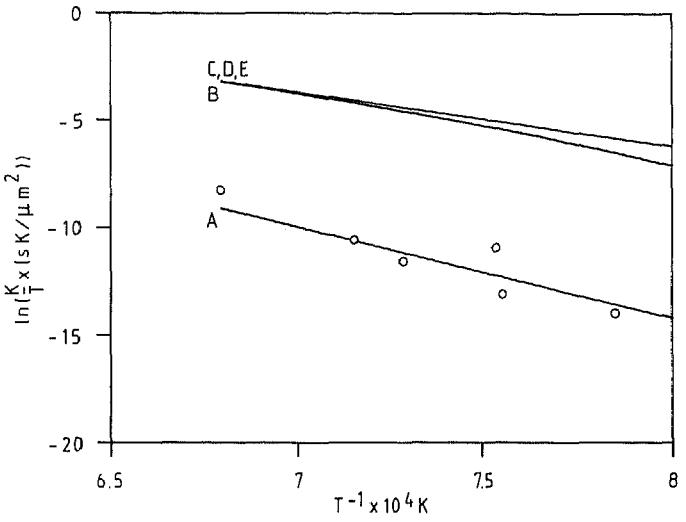

Figure 7. The calculated growth rate constant as a function of temperature at a $ZrCl_4$ input partial pressure of 10^{-3} atm for different input partial pressures of oxygen. Line A: P'_{O2}(input) = 10^{-4} atm, line B: P'_{O2}(input) = 10^{-8} atm, line C: P'_{O2}(input) = 10^{-12} atm, line D: P'_{O2}(input) = 10^{-16} atm, and line E: P'_{O2}(input) = 10^{-20} atm.

Hence, the experimental results can be understood assuming an oxygen concentration in the carrier gas of 10^4 ppm (i.e. typically 10^{-4} atm in the reactor). However, it is unlikely that such an amount of oxygen is present in the carrier gas. It is common to have an oxygen impurity level of 1 to 10 ppm [24].

Yet, if parabolic growth is assumed and the oxygen concentration in the carrier gas is on the order of 1 to 10 ppm, the predicted growth rate is too high, as discussed earlier. From these observations it may be concluded that the EVD layer may act as an oxygen selective membrane, and that only a small portion of the total oxygen flux through the EVD layer contributes to the actual growth. Hence, this might result in an increase of the oxygen partial pressure at the metal chloride side.

The ratio between the observed and the predicted growth rate is proportional to the conversion of transported oxygen to metal oxide. This ratio (i.e. conversion) increases with increasing temperature, and varies from a few tenth of a percent to a few percent typically [33]. This information can only be used in a qualitative way,

because the low conversion of oxygen will affect the actual oxygen partial pressure on the metal chloride side, and consequently the oxygen flux through the film. Besides, the assumption that solid state diffusion is rate limiting and that all other reaction rates are infinite can not be valid anymore. These observations suggest an EVD process which is determined by a combination of solid state diffusion and surface kinetics.

The increase in conversion with increasing temperature might be explained in terms of some limitations in the surface kinetics. However, at this stage this indistinctness of EVD growth can not be solved, because to our knowledge there are no reliable data concerning the surface kinetics between O_2 and $ZrCl_4$ present. In principle an EVD growth rate constant can be calculated by a numerical solution of the mass transport through the film and the kinetics at the surface provided that the required data are known. Consequently this calculated growth rate constant has to be compared with experimental data of EVD growth to verify as to whether the EVD growth is indeed controlled by a combination of solid state diffusion and surface kinetics.

It should be noted that the electron conductivity data used for these calculations were obtained from sintered YSZ samples [32]. It might be possible that the actual electron conductivity in the EVD layer differs from the electron conductivity data used in the calculations, e.g. due to the incorporation of chlorine or hydrogen during the EVD process, or grain boundary polarization phenomena, resulting in a lower electron conductivity of the YSZ. However, it is not very likely that this possible difference in electron conductivity can explain the discrepancies, as discussed.

4. MOCVD of TiS_2 thin film cathodes

4.1 PROCESS PARAMETERS AND MICRO STRUCTURE

In figure 8 the deposition rates for hot-wall depositions using 1.4 vol% HMDST and 0.25 vol% $TiCl_4$ at 7.5 and 20 mbar are presented. This figure shows that an increase of the pressure from 7.5 to 20 mbar does not affect the deposition rate.

XRD showed that all TiS_2 films above 0.5 μm consist of hexagonal TiS_2. The preferred orientation appeared to be a function of either temperature or film thickness. Strong preferred orientation with the c-axis parallel to the substrate surface was found in a 5.4 μm thick film deposited at 350°C and 20 mbar with HMDST, and in a 1.5 μm thick film deposited at 455°C with H_2S. Hence, in these samples the lithium conducting planes are oriented perpendicular to the substrate. Almost no preferred orientation was found in a 1.54 μm thick film deposited at 250°C with HMDST, while in a 0.5 μm thick film deposited at 357°C with H_2S the crystallites were found to have a preferred orientation with their conducting planes parallel to the substrate. Hence, strong preferred orientation with the c-axis parallel to the substrate surface is found in the thickest layers, or the ones deposited

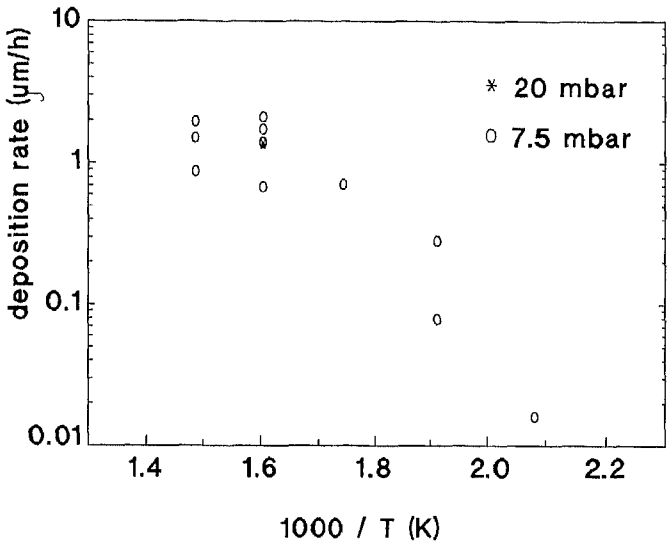

Figure 8. Deposition rates of TiS_2 for hot-wall depositions from 1.4 % HMDST and 0.25 % $TiCl_4$, at total pressures of 7.5 and 20 mbar, respectively.

at the highest temperatures, while the thinner layers, or the ones deposited at lower temperatures show either no preferred orientation, or a preferred orientation with the c-axis perpendicular to the substrate surface. Earlier observations also revealed improved orientation with increasing temperature or thickness [2,40].

In spite of the varying preferred orientations, all films showed a similar morphology. Only the film deposited at 207°C and 7.5 mbar with HMDST as sulphur precursor showed a different morphology (figure 9). Also TiS_2 deposited by Physical Vapor Deposition techniques exhibit a similar morphology. The reason why the morphology is almost independent of the deposition technique or deposition conditions is not yet clear.

The porosity of the films seems to be determined by the deposition conditions, and appears to decrease with increasing temperature or thickness.

4.2 ELECTROCHEMICAL PROPERTIES

Electrochemical measurements were performed on TiS_2-films deposited from HMDST at 7.5 mbar in a cold-wall reactor. Figure 10 shows the OCV of the cells as a function of the lithium content in the Li_xTiS_2-cathode. The OCV varies from 2.7 V for $x=0$ to 1.9 V for $x=1.0$, for both films. Figure 11 shows the thermodynamic enhancement factor, as derived from the OCV-curve, as a function of lithium content. It increases with lithium content from ± 5 to ± 50.

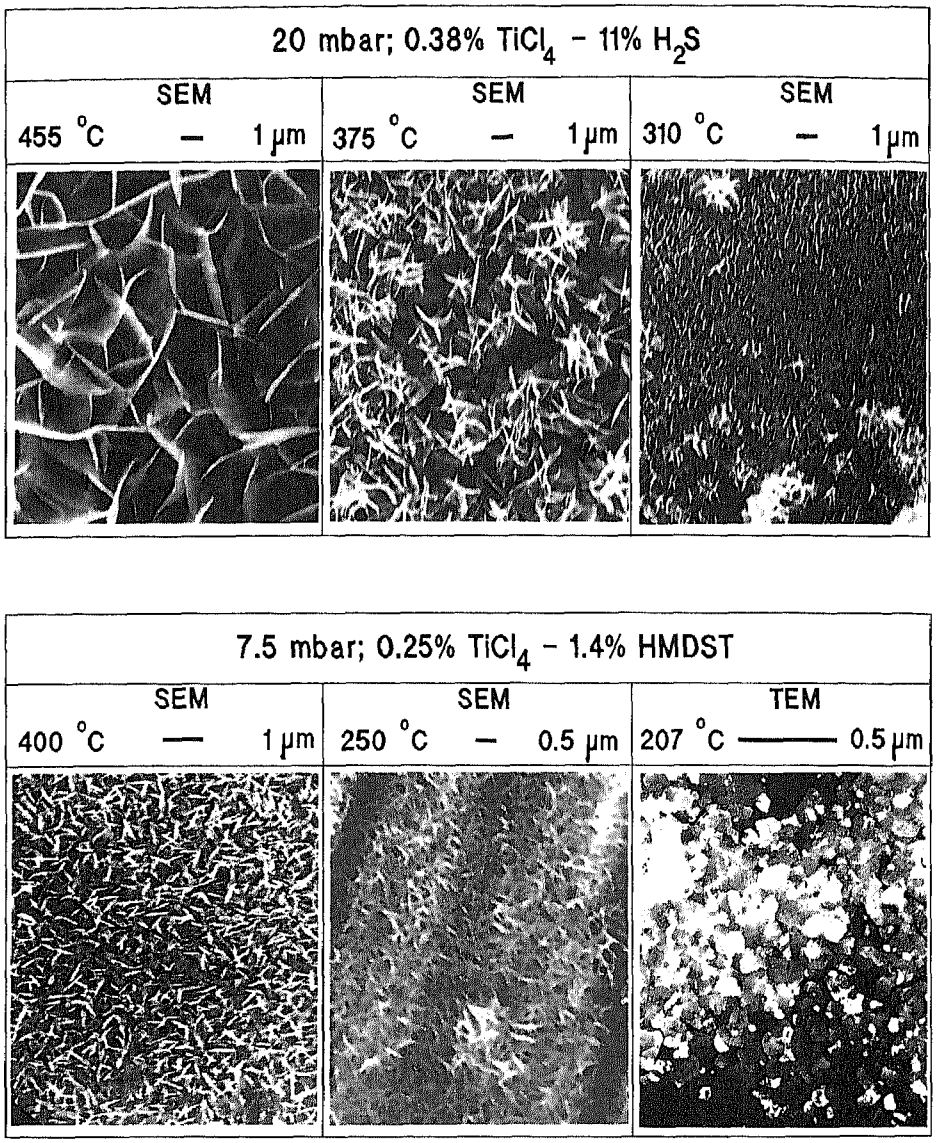

Figure 9. Morphology of (MO)CVD films of TiS_2.

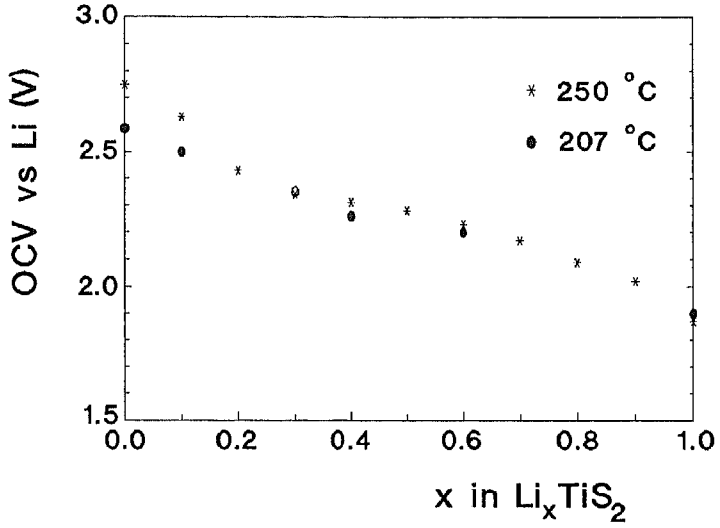

Figure 10. OCV of the cell Li_xTiS_2|1M $LiClO_4$ in PC|Li as a function of lithium content in TiS_2 films deposited at 207 and 250°C from HMDST and $TiCl_4$.

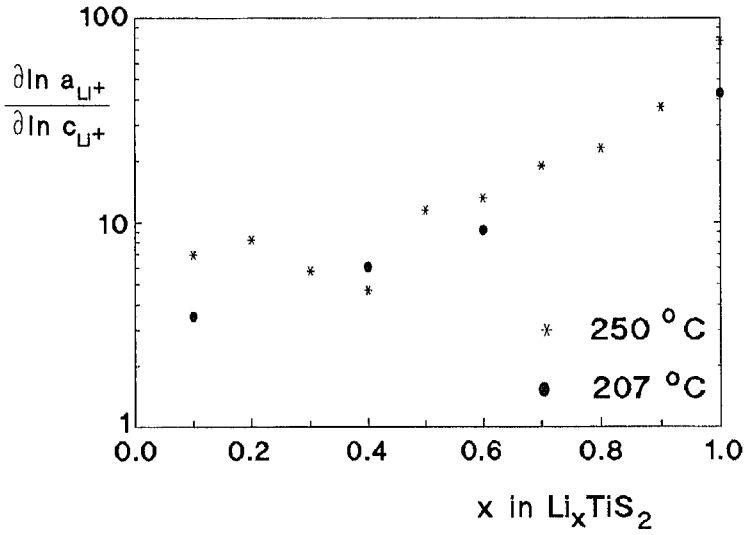

Figure 11. Thermodynamic enhancement factor as a function of lithium content in TiS_2 films deposited at 207 and 250°C from HMDST and $TiCl_4$.

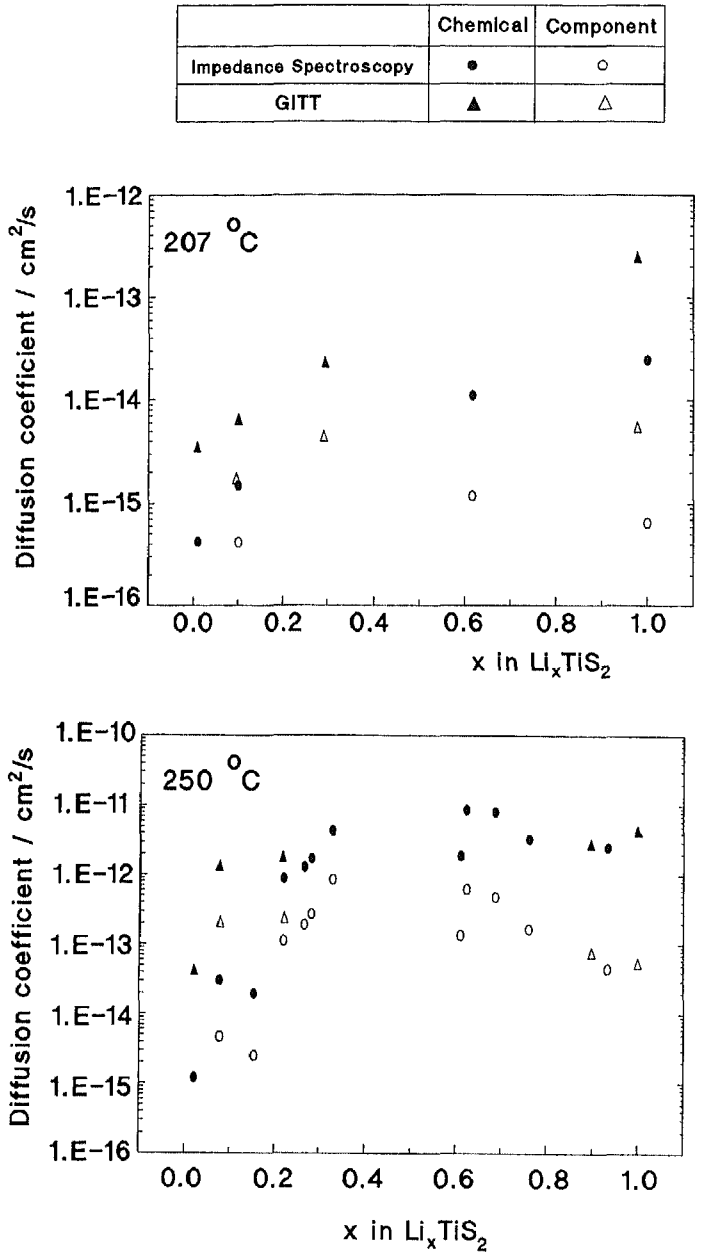

Figure 12. The chemical and component diffusion coefficients for lithium in the 207 and 250°C TiS_2 films as a function of lithium content.

Figure 12 shows the chemical and component diffusion coefficient as a function of lithium content, determined with GITT and IS. The lithium diffusion coefficients found are significantly lower than the lithium diffusion coefficient in pressed powder TiS_2, which is 5.6×10^{-9} cm^2/s. The slow rise of the lithium diffusion coefficient for $0\leq x\leq 0.4$, and decrease for $0.4\leq x\leq 0.9$ is in agreement with the behaviour found in single crystals [41,42], and in a thin film deposited by means of activated reactive evaporation [43]. The slight increase in the diffusion coefficient for $0.9\leq x\leq 1.0$, as shown in figure 12, is mainly due to the increase in the thermodynamic enhancement factor.

The lithium conduction of the 207°C sample is much lower than that of the 250°C sample. There are two possible explanations for this difference. One cause could be a difference in grain boundary polarization, because the lithium diffusion path crosses more grain boundaries in the 207°C film. The difference in lithium conductivity could also be caused by a difference in stoichiometry [41].

The diffusion coefficients in both films are lower than the ones found in single crystals or TiS_2 powder. This may be due to an error in the estimated current exchange area. In the calculations the current exchange area was approximated by the geometrical surface area of the films. However, for the 250°C film this value should be much smaller, as can be seen from its morphology. The calculated diffusion coefficient is inversely proportional to the square of the current exchange area. Hence, an inaccurate value for the current exchange area will lead to large errors in the calculated diffusion coefficients.

Figure 12 shows that there can be a considerable difference between results of IS and GITT. This difference may be the result of either the interpretation of the impedance spectra or polarization effects due to porosity of the films.

IS only yields reliable results in the case of well interpretable spectra. An example of such a spectrum is shown in figure 13. This spectrum can be readily fitted by the physically well justified equivalent circuit R_1Q_1pRsTs, where R^{-1} represents the lithium conduction in the electrolyte, Q_1 a CPE element related to charge transfer phenomena, R_1 the charge transfer resistance, and T the finite-length diffusion through a medium with a reflective boundary [42]; s and p stand for series and parallel, respectively. In other cases data have been obtained from only that small part of the spectrum, which has a slope of 45°, and which has been interpreted as the 45° degrees slope of a T-element.

Polarization effects due to porosity may give erroneous results with both IS and GITT. In the case of thin film mixed conductors, the two measurement techniques are essentially based on the same principle: the mathematical description of the polarization of a finite-length mixed conductor due to lithium diffusion. The only difference is that IS describes the response to an AC current as a function of frequency, and GITT the response to a DC current pulse. It is clear that polarization due to porosity can cause serious variations in the values of the lithium diffusion coefficient determined with either method.

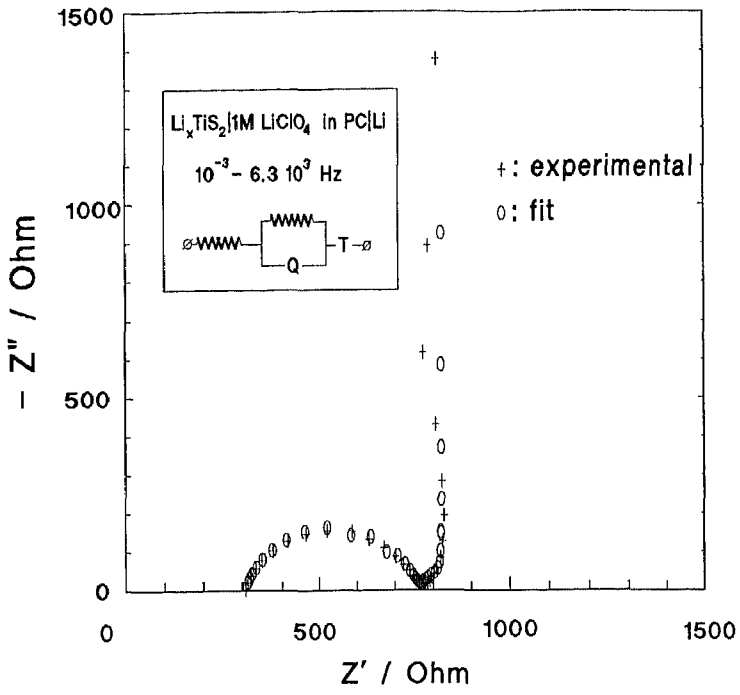

Figure 13. Impedance spectrum of the cell Li_xTiS_2 | 1M $LiClO_4$ in PC | Li.

5. Conclusions

5.1 EVD GROWTH OF YSZ

The temperature dependence of the experimental parabolic growth rate constant of YSZ was used to verify whether the growth rate is limited by solid state diffusion. The high observed apparent activation energy of 4.4 eV of the EVD growth justifies the assumption that solid state mass transport through the film is the rate limiting step.

The calculated parabolic growth rate constant is higher than the experimental one. Hence, either the material constants used for the calculations are not valid for the EVD layer, or the growth rate mechanism is more complex then originally assumed.

Taking into account that traces of oxygen at the metal chloride side have a large influence on the theoretical parabolic growth rate constant, the experimentally determined parabolic growth rate constant can be understood if the presence of 10^4 ppm of oxygen in the carrier gas at the metal chloride side is assumed.

From the observations it might be concluded that the EVD layer acts as an oxygen pump and that only a small portion of the oxygen actually reacts with the metal chloride to form the metal oxide.

In principle this complex mass transport phenomenon can be solved numerically. However, at this stage there are not enough data present to solve the equations. Hence, more experimental work concerning the kinetics of EVD and CVD using $ZrCl_4$ and O_2 as reactants has to be done in order to obtain a full model which can predict the EVD growth rate of YSZ.

5.2 MOCVD OF TIS_2

The preferred crystallite orientation in MOCVD TiS_2-films seems to be a function of either temperature or film thickness. The overall chemical diffusion coefficient for lithium in thin-film TiS_2 is lower than in powder TiS_2 and depends on the porosity of the film.

Furthermore, there is a need of accurate models for and microstructural analyses of porous, rough and anisotropically conducting mixed conducting thin-film electrodes. These will allow a systematic optimization of the electrode properties and a correct interpretation of the IS and GITT results.

6. References

[1] A.O. Isenberg, Thin Film Battery/Fuel Cell Power Generating System, Report ERDA, Contract EY-76-C-03-1197, Westinghouse Electric Corporation, Pittsburgh, PA, (1978).

[2] K. Kanehori, K. Matsumoto, K. Miyauchi and T. Kudo, Solid State Ionics 9/10 (1983), 1445.

[3] F.S. Galasso, Chemical Vapor Deposited Materials, CRC Press Inc., Boca Raton, FL, (1992).

[4] K.E. Spear, Pure Appl. Chem. 54 (1982), 1297.

[5] C.H.J. van den Brekel, Philips Res. Repts. 32 (1977), 118.

[6] C.H.J. van den Brekel and J. Bloem, Philips Res. Repts. 32 (1977), 134.

[7] R.A. Bauer, F.E. Kruis, P. van der Put, B. Scarlett and J. Schoonman, KONA 8 (1990), 145.

[8] W.R. Cannon, S.C. Danforth, J.H. Flint, J.S. Haggerty and R.A. Marra, J. Am. Ceram. Soc. 65 (1982), 324.

[9] P. van der Straten and G. Verspui, Philips Tech. Rev. 40 (1982), 204.

[10] A. Caputo, W. Lackey and I. Wright, Proc. 9th Int. Conf. on CVD, Electrochemical Society, Pennington, NJ, (1984), 782.

[11] M. Basche, R. Fanti and F. Galasso, Fibre Sci. Tech. 1 (1968), 19.

[12] J. Camahort, J. Compos. Mater. 2 (1968), 104.
[13] B. Jacob, R. Bourdeau and F. Galasso, Fibre Sci. Tech. 2 (1969), 243.
[14] C.F. Wan and K.E. Spear, Proc. 6th Int. Conf. on CVD, Electrochemical Society, Princeton, NJ, (1977).
[15] P.F. Freund and K.E. Spear, J. Less Common Met. 60 (1978), 185.
[16] N.B. Hanney, Treaties on Solid State Chemistry, Plenum Press, New York, NY, (1975), Vol. 5.
[17] A.O. Isenberg, Proc. Symp. Elec. Mat. and Proc. for Eng. Conv. and Stor., Electrochemical Society, Princeton, NJ, 77-6 (1977), 572.
[18] U.B. Pal and S.C. Singhal, J. Electrochem. Soc. 137 (1990), 2937.
[19] M.F. Carolan and J.N. Michaels, Solid State Ionics 37 (1990), 189.
[20] J.P. Dekker, N.J. Kiwiet and J. Schoonman, Solid Oxide Fuel Cells, S.C. Singhal (ed.), Electrochemical Society, Pennington, NJ, (1989), 57.
[21] N.J. Kiwiet and J. Schoonman, Proc. 25th Int. Soc. Energy Conv. Eng. Conf., Vol. 3, P.A. Nelson et al. (eds.), AIChE, New York, NY, (1990), 240.
[22] J. Schoonman, J.P. Dekker, J.W. Broers and N.J. Kiwiet, Solid State Ionics 46 (1991), 299.
[23] Y.S. Lin, L.G.J. de Haart, K.J. de Vries and A.J. Burggraaf, J. Electrochem. Soc. 137 (1990), 3960.
[24] Y.S. Lin, Chemical and Electrochemical Vapor Deposition of Zirconia-Yttria Solid Solutions in Porous Ceramic Media, PhD. Thesis, University of Twente, Enschede, The Netherlands, (1991), Ch.6.
[25] H. Komiyama, T. Osawa, Y. Shimogaki, N. Wakita, M. Mianamiyama and T. Ueoka, Proc. 10th Int. Conf. on CVD, Electrochemical Society, Pennington, NJ, (1987), 1119.
[26] J.P. Dekker, P.J. van der Put, H.J. Veringa and J. Schoonman, Ceramics Adding the Value, Vol.1, M.J. Bannister (ed.), AUSTCERAM 92, CSIRO Publications, Melbourne, (1992), 787.
[27] T. Kimura and T. Kojima, J. de Physique IV (C2) (1991), Vol. 1, C2-103.
[28] J.H.D. Rebello, D.L. Straub, V.V. Subramaniam, E.K. Tan, S.A. Dregia, B.L. Preppernau and T.A. Miller, Mater. & Manuf. Proc. 6 (1991), 501
[29] C. Wagner, Z. Physik. Chem. 32 (1936), 447.
[30] P.Kofstad, High Temperature Corrosion, Elsevier Applied Science Publishers LTD, Amsterdam, (1988), Ch.6.
[31] J.P. Dekker, V.E.J. van Dieten and J. Schoonman, Solid State Ionics 51 (1992), 143.
[32] J.M. Park and R.N. Blumenthal, J. Electrochem. Soc. 136 (1989), 2867.
[33] J.P. Dekker, V.E.J. van Dieten and J. Schoonman, submitted to J. Electrochem. Soc. (1992).
[34] G. Eriksson, Chemica Scripta 8 (1975), 100.
[35] G. Eriksson and K. Hack, Chemsage (Computer program), GTT GmbH, Germany, (1991).

[36] JANAF Thermochemical Tables, 2nd edition, D.R. Stull and H. Prophet (eds.), U.S. Government Printing Office, Washington DC, (1971).
[37] J.P. Dekker, V.E.J. van Dieten and J. Schoonman, accepted for Proc. 5th Int. Conf. on the Sci. and Techn. of Zirconia, S.P.S Badwal, M.J. Bannister and R.H.J. Hannink (eds.), Technomic Publishing Company, Lancaster, PA, to be published in 1993.
[38] A.A. van Zomeren, J.H. Koegler, J. Schoonman and P.J. van der Put, Solid State Ionics 53-56 (1992), 333.
[39] W. Weppner and R.A Huggins, J. Electrochem. Soc. 124 (1977), 1569.
[40] S. Kikkawa, R. Shimanouchi-Futagami and M. Koizumi, Appl. Phys. A 49 (1989), 105.
[41] K. Kanehori, F. Kirino, T. Kudo and K. Miyauchi, J. Electrochem. Soc. 138 (1991), 2216.
[42] K. West, T. Jacobsen, B. Zachau-Christiansen and S. Atlung, Extended Abstract, 32 nd I.S.E. Meeting, Dubrovnik, I.S.E. (1981), 11.
[43] D. Zehnder, C. Deshpandey, B. Dunn and R.F. Bunshah, Solid State Ionics 18&19 (1986), 813.
[44] I.D. Raistrick, J.R. Macdonald and D.R. Franceschetti, Impedance Spectroscopy, J.R. Macdonald (ed.), Wiley, New York, NY, (1987), 59.